Journal of Biomedical Optics

SPIEDigitalLibrary.org/jbo

Investigation of transport dynamics in oleic acid–induced transdermal drug delivery by two-photon fluorescence microscopy: an *ex-vivo* study of mouse skin

Te-Yu Tseng
Hsun-Chia Hsu
Chiu-Sheng Yang
Tsung-Hua Tsai
Chen-Yuan Dong

SPIE

Investigation of transport dynamics in oleic acid–induced transdermal drug delivery by two-photon fluorescence microscopy: an *ex-vivo* study of mouse skin

Te-Yu Tseng,[a*] Hsun-Chia Hsu,[a*] Chiu-Sheng Yang,[a] Tsung-Hua Tsai,[b] and Chen-Yuan Dong[a,c,d]
[a]National Taiwan University, Department of Physics, Room 530, Taipei 106, Taiwan
[b]Far Eastern Memorial Hospital, Department of Dermatology, New Taipei City 220, Taiwan
[c]National Taiwan University, Center for Quantum Science and Engineering, Taipei 106, Taiwan
[d]National Taiwan University, Center for Optoelectronic Biomedicine, Taipei 106, Taiwan

Abstract. Transdermal drug delivery, transporting the drug molecules through epidermis to dermis, has been extensively investigated but not studied in dynamic detail. The objective of this study is to monitor the dynamical changes of drug permeation and that of polarization of skin tissue with oleic acid treatment. We utilize two-photon fluorescence microscopy (TPM) to investigate the dynamics of transdermal drug delivery in skin excised from the abdominal region of euthenized nude mice with sulforhodamine B (SRB) modeling as a drug and Laurdan serving as a polarity indicator. The treatment of oleic acid increases the permeation rate of SRB, quickly reaching to the steady state of permeation. Increases in polarity within the skin tissue (in both intercellular and intracellular region of stratum corneum) are observed in SRB permeation enhanced by oleic acid treatment. TPM has successfully demonstrated the ability to study spatial distribution of transport dynamics in oleic acid-enhanced transdermal delivery. [DOI: 10.1117/1.JBO.18.9.096016]

Keywords: stratum corneum; transdermal drug delivery; two-photon fluorescence microscopy; general polarization; oleic acid; Laurdan; sulforhodamine B.

Paper 130056RR received Jan. 31, 2013; revised manuscript received Aug. 22, 2013; accepted for publication Aug. 28, 2013; published online Sep. 25, 2013.

1 Introduction

Oral administration and subcutaneous injection are the common methods for drug delivery. Oral delivery is convenient in the case where repeated treatments are needed. However, this approach is limited in first-pass metabolism by the gastrointestinal tract. On the other hand, subcutaneous injection eliminates enzymatic degradation of the gastrointestinal tract. However, this type of delivery places psychological stress on patients to whom the use of needle induces fear. In comparison, transdermal drug delivery is advantageous in that it is noninvasive and able to maintain sustained delivery of therapeutic agents. Therefore, transdermal delivery represents an attractive alternative to traditional delivery strategies. The key step in transdermal delivery is to transport the drug molecules through the epidermis to the capillary-rich dermis for drug absorption. The major challenge of this methodology is to make drug efficiently penetrate the stratum corneum (SC), the outermost layer of skin composed of corneocytes.[1]

Mechanisms of transdermal drug delivery have been studied for the past three decades as a number of methods have been developed to reduce the skin barrier safely and reversely for drug penetration.[2] Among them, the use of a chemical enhancer is one of the well-studied approaches.[3] An appropriate chemical can enhance drug transport across the skin by interacting with the skin components and altering the highly ordered lipid-bilayer structure of cellular membranes. Among the different chemical enhancers used, oleic acid is one of the fatty acids commonly used. Oleic acid has the unique property in that it can disturb the lipid structure of the SC to increase the lipid fluidity, resulting in improving transdermal drug efficacy.[4]

Conventionally, transdermal delivery has been observed through particles flux measurement by high-performance liquid chromatography capable of quantitatively analyzing molecular component of liquid mixture. Such flux measurement, however, does not provide structural or morphological information of the dynamic changes of skin during the transdermal delivery process. In contrast, two-photon fluorescence microscopy (TPM) allows real-time imaging of the permeation process, providing time-dependent structural and morphological changes in the SC. The additional information will enable a better understanding of the transdermal permeation process and provide additional insights into the time scale of dynamic processes during transdermal delivery. Previously, TPM has been utilized to study the three-dimensional (3-D), steady-state spatial distribution of the hydrophilic- and hydrophobic-modeled drugs in human skin under the oleic acid enhancement *in vitro*.[5,6] The chemical-induced changes in the transport properties and transdermal permeability of the permeant were measured and quantified.[5] However, the dynamic processes leading to the establishment of equilibrium in the chemical permeation process on skin structure remains to be clarified.

In this study, sulforhodamine B (SRB) was used as the model drug molecule in studying the dynamic processes of transdermal delivery. In addition, Laurdan, an amphiphilic polarity-sensitive

*These authors contributed equally to this work.

Address all correspondence to: Tsung-Hua Tsai, Far Eastern Memorial Hospital, Department of Dermatology, New Taipei City 220, Taiwan. Tel: + 886 2 89667000 4287; E-mail: tsaitsunghua@yahoo.com.tw; Chen-Yuan Dong, National Taiwan University, Department of Physics, Taipei 106, Taiwan. Tel: +886 2 3366 5155; E-mail: cydong@phys.ntu.edu.tw

0091-3286/2013/$25.00 © 2013 SPIE

fluorescence dye, was used for monitoring the changes of the local polarity within the skin's microenvironment.[7] Finally, oleic acid, which acted as the chemical permeation enhancer, was used for investigating dynamics of transdermal delivery. Fluorescence of both SRB and Laurdan was excited and their distribution in the skin visualized through the use of TPM. We acquired 3-D, two-photon images of fluorescent dyes for structural reconstruction of *ex-vivo* mouse skin treated with and without the chemical enhancer oleic acid. Time-lapse images were obtained and analyzed for the transport dynamics of transdermal delivery. In addition to revealing the mechanism of the transdermal delivery of SRB, our results also demonstrated that the two-photon microscopy was an excellent technique to monitor the dynamical transport of transdermal permeation.

2 Materials and Methods

2.1 *Laurdan and Generalized Polarization Function*

Laurdan (Molecular Probes, Eugene, OR) can be effectively used as a probe for detecting membrane fluidity as it can be aligned parallel to the hydrophobic tails of the phospholipids in the membrane.[8,9] Laurdan also has the unique spectral properties in which its fluorescence emission peaks change as a function of environmental polarity. The emission peak wavelength of Laurdan is about 440 nm in nonpolar solvent and shifts to 490 nm in polar solvent. This effect is attributed to greater charge separation in polar solvent resulting in increased dipole moment.[9] Therefore, as the packing of the phospholipids in the membrane becomes increasingly disordered, the membrane will become more permeable to water, exposing the Laurdan on the membrane to a more polar environment and leading to its emission peak wavelength to shift from 440 nm towards 490 nm. To quantify the environmental polarity with Laurdan fluorescence, it is convenient to define a generalized polarization (GP) function as

$$\mathrm{GP} = \frac{I_{440\ \mathrm{nm}} - I_{490\ \mathrm{nm}}}{I_{440\ \mathrm{nm}} + I_{490\ \mathrm{nm}}}. \quad (1)$$

According to this definition, a microenvironment of more ordered membrane packing and less water permeability would result in a GP value closer to 1. On the other hand, a more disordered membrane packing and hence greater permeability to polar water molecules would shift the GP value closer to -1.[8]

2.2 *Oleic Acid and SRB*

The chemical enhancer oleic acid (Sigma Aldrich, St. Louis, MO) is a *cis*-unsaturated fatty acid with a single double bond. The kinked structure in oleic acid limits the ability of phospholipids to pack closely, resulting in a low membrane melting temperature and an increase in skin permeability.[10–13] Previous research found that *cis*-unsaturated fatty acid partitions the membrane into a fluid-like phase, while trans-unsaturated and saturated preferentially partition into a solid-like domain.[14] For this study, the polar molecule SRB (Molecular Probes) was used and modeled as the hydrophilic drug. As a model drug, SRB has a number of advantages. First, its relative small molecular weight of 559 Da resembles that of many drug molecules. Furthermore, the water solubility of SRB enables it to be a hydrophilic model. Finally, with respective single-photon excitation and emission maxima of 565 and 586 nm, SRB can be excited under two-photon absorption for microscopic imaging studies.[5]

2.3 *Permeating Solution Preparation*

The contents of the permeating solutions for the specimens treated without and with oleic acid are described as below. For the specimens without oleic acid, the permeating solutions consisted of 0.1 ml of 3.3 mM Laurdan [in dimethyl sulfoxide (DMSO)], 0.4 ml of 0.1 mM SRB stocking in phosphate-buffered saline (PBS) and ethanol (1:1 v/v solution), 3.1 ml PBS (Sigma Aldrich), and 6.2 ml ethanol. In the specimens treated with oleic acid, the permeating solutions have the same composition as described above with the addition of 0.3 ml oleic acid (3% v/v). The addition of Laurdan in the both groups was intended to help maintain the concentration of Laurdan inside the skin specimen, preventing the reverse permeation of pretreated Laurdan from the SC.

2.4 *Ex-vivo Skin Specimen Preparation*

Skin excised from the abdominal region of a euthenized nude mouse was stored at −20°C and used within 2 weeks of experimentation. On the day of the experiment, the skin was first thawed at room temperature for 20 min and cut into 1 cm^2 pieces for processing. Prior to image acquisition, the skin was soaked in 0.033 mM Laurdan in PBS solution (3.3 mM stock in DMSO) for 14 h. At the end of the treatment period, the skin was rinsed with PBS and cleaned with tissue paper. Subsequently, the specimen was placed flatly on a cover glass, with its edges sealed by clay, exposing only the epidermal surface of the skin to the permeation solutions. The clay-sealed specimen was then placed at the center of a glass bottom dish (MatTek Corporation, Ashland, MA) and placed on the microscope for imaging.

2.5 *Two-Photon Fluorescence Microscopy*

The optical setup of TPM used in this study is similar to one previously reported.[15] Images were obtained by the use of our home-built, multiphoton laser scanning microscope system coupled with the pulsed, femtosecond, titanium: sapphire laser (Tsunami, Spectra-Physics, Mountain View, CA). A 20× water immersion objective (N.A. 0.75, W.D. 0.35 mm, Plan Fluor, Nikon, Japan) was used for focusing the laser source at wavelength of 780 nm. The on-sample laser power was 15 to 40 mW and the fluorescence emission signal was collected in the epi-illuminated geometry. For fluorescence imaging, the main dichroic mirror (700DCSPXRUV-3p, Chroma Technology, Brattleboro, VT) which reflected the excitation source into the focusing objective, blocked the incident laser and allowed the collected fluorescence emission to pass. For multichannel detections, two dichroic mirrors (555DCXR, 470DCXR, Chroma Technology, Brattleboro, VT) and three band-pass filters (590/80, 490/40, 440/40, Chroma Technology) divided the emission fluorescence into three respective channels of 550 to 630 nm, 470 to 510 nm, and 420 to 460 nm for detection by the photomultiplier tubes (R7400P, Hamamatsu, Hamamatsu City, Shizuoka, Japan). A motorized translation stage (H101, Prior Scientific Instruments, Cambridge, UK) was used to acquire the multiphoton images at different depths for 3-D image acquisition.

2.6 *Imaging Acquisition and Data Analysis*

After placing the surface of the skin specimen under the microscope, we added the permeating solution with total volume of 10 ml onto the skin specimen and started imaging acquisition. During experiments, the skin specimen and the objective were immersed in the permeating solution and were kept in hermetical space sealed by plastic film for maintaining all concentrations of components in the solution.

Total thickness of the epidermis in the mouse skin is about 30 μm.[16] The outer layer of the epidermis, the SC, is about 10-μm thick. The underlying layers, stratum granulosum and stratum spinosum, extend about 5 μm. The innermost part of the epidermis is called the basal layer. In each experiment, images of 512×512 pixels (220×220 μm^2) at the depth of 3 μm apart were acquired for the acquisition of each 3-D image stack. Due to the unevenness of the skin surface, we selected three random 150×150 pixels (65×65 μm^2) squared regions where the skin surface showed relative flatness from the entire image for analyzing the overall permeation on SC. Time-lapse images in 3-D were acquired for 240 min. Three specimens in each group were analyzed for average SRB distribution and GP mapping.

We analyzed depth-resolved images at different time intervals and obtained SRB intensity as well as the corresponding GP values by the use of ImageJ (U.S. National Institutes of Health, Bethesda, Maryland) and IDL (Exelis Visual Information Solutions, Boulder, Colorado). Note that in GP imaging, simultaneous measurement of Laurdan fluorescence at 440 and 490 nm is required. However, in imaging below the skin surface, tissue scattering can affect the relative detection efficiency of these two wavelengths. Specifically, 440-nm photons will scatter more significantly than 490-nm photons, resulting in distorted determination of GP values. We circumvented this problem by normalizing the intensity in each channel by dividing each pixel of the raw image by the intensity by the average of top 10% intensity values of each image. In this manner, the effect of wavelength-dependent scattering can be eliminated.

In addition to analyzing the overall permeation on SC across the entire image, we also focused on the intercellular phospholipid regions (IPR) as this continuous and porous structure interacts with most of clinical enhancers[10] and was the main pathway for transdermal permeation.[17] In the specific analysis of the IPR, about 10-pixel-wide boundaries surrounding corneocytes of the selected images were averaged to obtain the time-dependent permeation of SRB molecules and changes in GP values.

3 Results and Discussion

3.1 *Imaging of SRB Intensity and GP Distributions*

To investigate the effects of the oleic acid on the transdermal permeation of SRB molecules, we acquired depth-resolved images for skin specimens with and without the addition of oleic acid at different time points. Both *en face*, 3-D, and cross-sectional imaging were performed to visualize the transdermal delivery of SRB molecules and changes in GP values. The respective 3-D SRB fluorescence image stacks of skin specimens without and with oleic acid treatment for 80 min is shown in Figs. 1(a) and 1(b). The calibration bar represents photon count for SRB images. The corresponding 3-D GP distributions are shown in Figs. 1(c) and 1(d). Qualitatively, these images show that oleic acid enhances SRB molecules permeating across

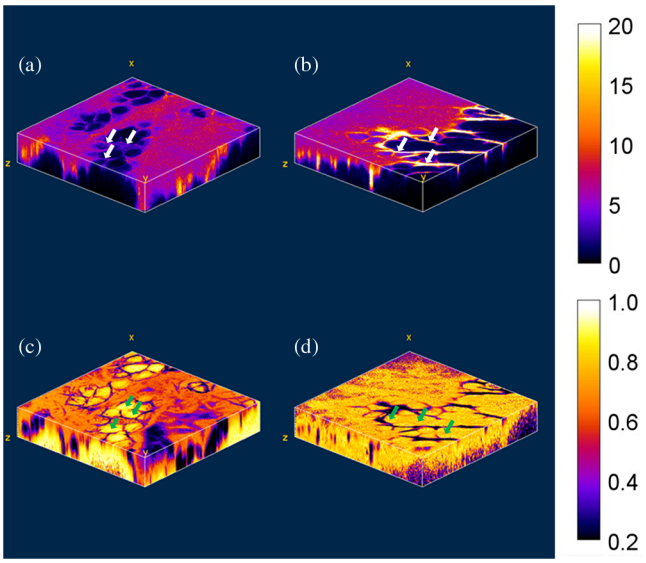

Fig. 1 Three-dimensional (3-D) sulforhodamine B (SRB) projections of skin specimens without (a) and with treating oleic acid for 80 min (b). 3-D generalized polarization (GP) projections of skin specimens without and with treating oleic acid for 80 min are presented in (c) and (d), respectively. White arrows point on intercellular phospholipid regions (IPRs), and green arrows point on intracellular regions. Y–Z section represents the cross-sectional view. The sizes of each stack are 220 (x-axis) $\times$ 220 (y-axis) $\times$ 45 μm^3 (z-axis). The calibration bar represents photon counts or GP values.

the skin tissue especially in IPR (white arrow) and makes intracellular regions (green arrows) became more polar.

To perform further analysis, representative cross-sectional images of SRB intensity and GP-resolved images at four different time intervals [20 (without oleic acid)/30 (with oleic acid), 80, 140, and 240 min] and depths (0, 6, 15, and 21 μm) are shown in Figs. 2 and 3, respectively. Since the skin surface is uneven, we defined the skin surface as the depth (0 μm) at which maximum SRB intensity was measured. This approach was previously used[5] and since images from all specimens are processed in the same way, comparison between the various groups can be made. The SRB intensity images for a skin specimen without and with oleic acid treatment are shown in Figs. 2(a) and 2(b). Qualitatively, these images show that SRB is present in greater amount in the oleic acid treated specimens as SRB fluorescence is higher in both intercellular (white-banded regions) and intracellular (green arrow) regions as compared to the specimens untreated with oleic acid. As mentioned in Sec. 2.6, white-banded regions defined as IPR are about 10-pixel-wide boundaries surrounding corneocytes of the selected images. Intracellular regions (green arrow) are inner parts of corneocytes in the selected images. In both white-banded regions and intracellular (green arrow) regions, the averaged SRB signal was determined by summing photon counts in all pixels divided by the total pixel number within the regions of interest. For example, in the case of Fig. 2 at a time point of 80 min and depth of 6 μm, the average SRB of IPR (white-banded regions) and the intracellular regions (green arrow) are 4.0 and 1.5 in the group without oleic acid, whereas those values are 8.7 and 4.5 in the oleic acid group. This observation is indicative of the fact that oleic acid enhances the permeation of SRB molecules in the transdermal delivery process. In addition, we also mapped the temporal change of GP

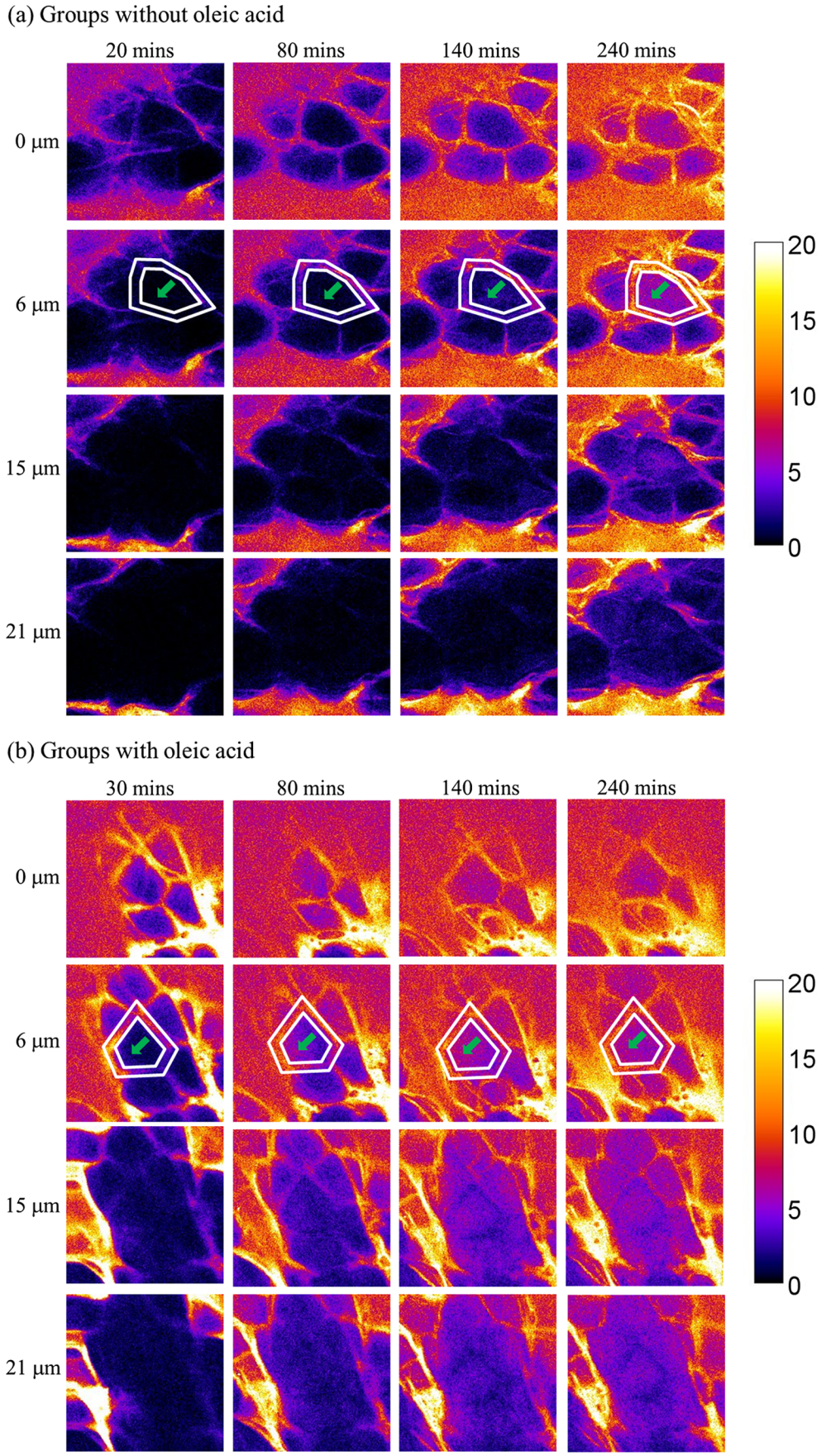

Fig. 2 SRB intensity images of a representative region at different depths and time points for the groups without (a) and with (b) oleic acid. White-banded regions present IPRs, and green arrows point on intracellular regions. The dimension of each image is 65 (x-axis) × 65 (y-axis) μm^2. The calibration bar represents photon counts.

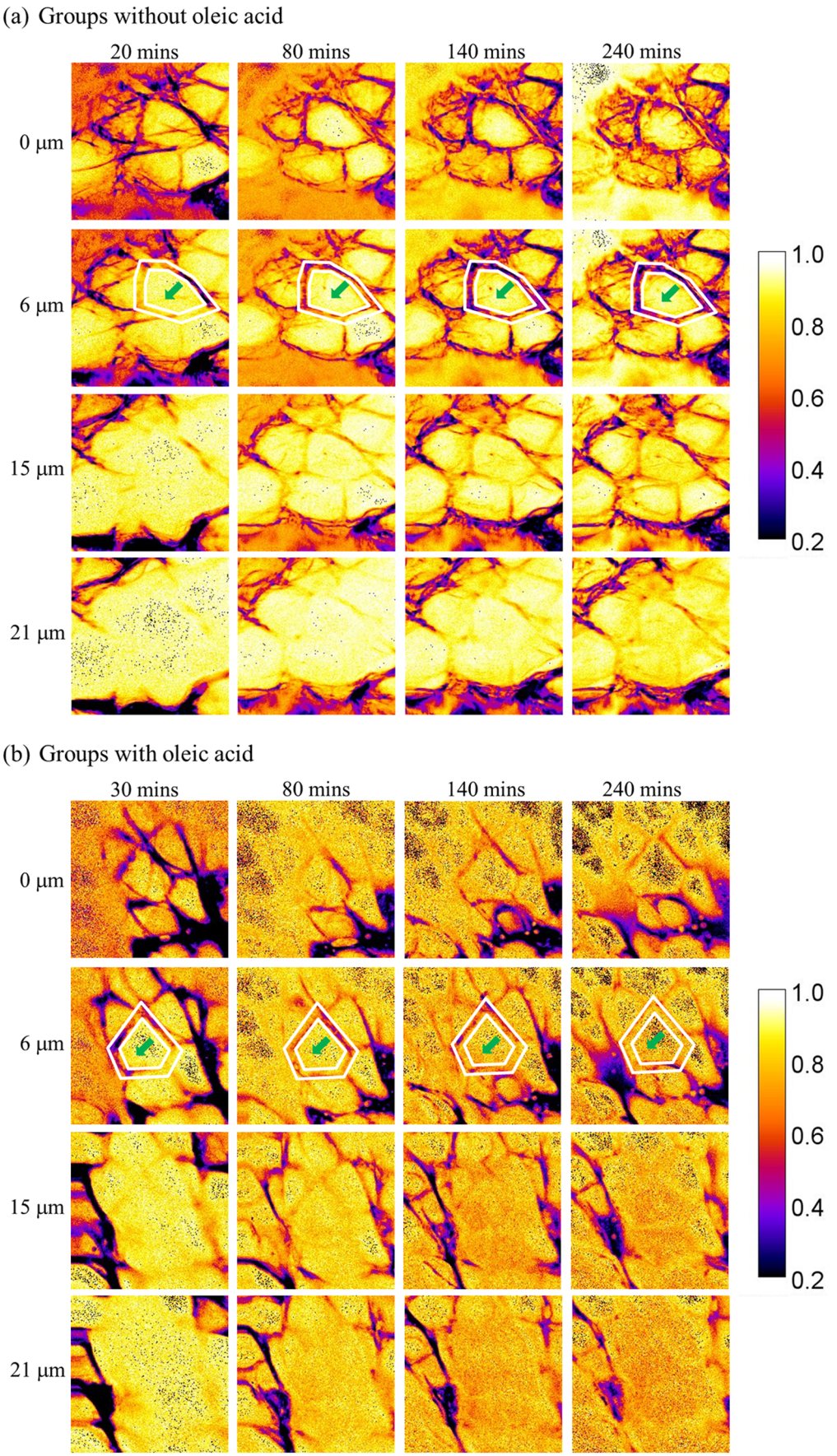

Fig. 3 The corresponding GP value of Figs. 2(a) and 2(b) at the same depths and time points shown in (a) without oleic acid and (b) with oleic acid, respectively. White-banded regions present IPRs, and green arrows point on intracellular regions. The calibration bar represents GP value.

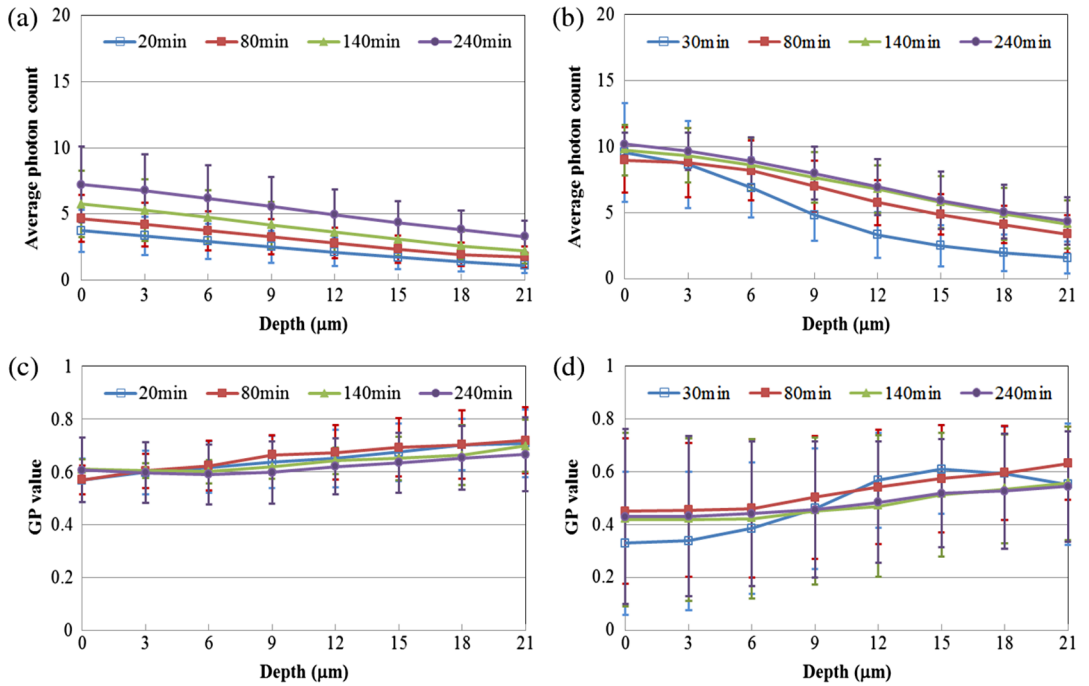

Fig. 4 Quantifications of average SRB intensity and GP values for the overall permeation on SC across the entire image. Depth-resolved and time-lapse SRB intensity for the groups without and with oleic acid are, respectively, shown in (a) and (b). *X*-axis is the depth of skin in micrometers and *Y*-axis is the average photon count. (c) and (d) show the results of respective GP values, respectively. *X*-axis is the depth of skin in micrometers and *Y*-axis is the GP value. Open squares, dark squares, triangles, and circles represent the results at time points of 20 (without oleic acid)/30 (with oleic acid), 80, 140, 240 min, respectively.

distribution to trace changes of cutaneous polarity (Fig. 3). We found that at the beginning of the imaging experiments, lower GP values were found in IPR than the intracellular regions. For example, in the case of Fig. 3 at time point of 80 min and depth of 6 μm, the average GP values of IPR (white-banded regions) and the intracellular regions (green arrow) are 0.51 and 0.88 in the group without oleic acid, whereas those are 0.68 and 0.83 in the group with oleic acid. Comparing GP values between the group without and with oleic acid [Figs. 3(a) and 3(b)], we found the GP values of the intracellular regions decreased and the GP distribution became homogeneous with time in the group with oleic acid while slight changes remained in the group without oleic acid. For example, at the depth of 6 μm, the average GP values of the intracellular regions are 0.86, 0.83, 0.78 and 0.76 at the four time points (30 to 240 min) in the group with oleic acid; however, the average GP value only change from 0.88 to 0.85 (20 to 240 min) in the group without oleic acid (Fig. 3). At the same depth, the average GP values of IPR increased from 0.63 to 0.72 with time in the group with oleic acid, which become closer to those of the intracellular regions and lead to a homogeneous distribution of GP. However, in the group without oleic acid, the average GP values of IPR decreased from 0.54 to 0.43 with time, which are different from those of the intracellular regions (Fig. 3). The GP mapping indicated that oleic acid affects the polarity of skin tissues and makes skin tissues more accessible to polar molecules.

As discussed previously,[5] when added to the skin surface, the kink in the structure of oleic acid would disrupt the skin membrane and enhance the permeation of hydrophilic molecules such as water and SRB. Similarly, GP value in the IPR region is expected to decrease corresponding to increased polarity. However, the skin surface is heterogeneous in structure and the GP values may vary in response to the addition to oleic acid. The above discussions correspond to the results of Figs. 2 and 3. A more precise result of the effect of GP in IPR region due to oleic acid (discussed below) indicate that in general, GP in the IPR region decreases in response to oleic acid, indicating that oleic acid eases the permeation of hydrophilic molecules there.

3.2 *Quantifications of SRB Intensity and GP Values*

For studying the dynamics of SRB permeation in transdermal delivery, quantifications of time-lapse SRB intensity and GP values as functions of depths were performed. In each group, three specimens were used to obtain average values of SRB intensity and GP values. The analysis we performed analyzed both SRB intensity and GP values across entire images and in the intercellular region.

In the analysis across the entire image, we averaged the both SRB and GP from selected regions of three specimens in both skin groups and plotted the general average intensity curves function of skin depth at four time points. Figs. 4(a) and 4(b), respectively, show the plots of average SRB results in the groups without and with oleic acid. The corresponding plots of average GP values at the same depths and time points are also present in Figs. 4(c) and 4(d). From Fig. 4(a), we observed that the depth-resolved SRB intensities of the group without oleic acid gradually increased with time even at 240 min after SRB permeation. However, Fig. 4(b) shows that <140 min was needed to reach the steady state of SRB permeation in the group with oleic acid. On the other hand, Fig. 4(c) indicates a slight decrease in GP function of skin depth at the four time points in the group without oleic acid, indicating that the skin polarity had changed, a result most likely due to the additional permeation of aqueous

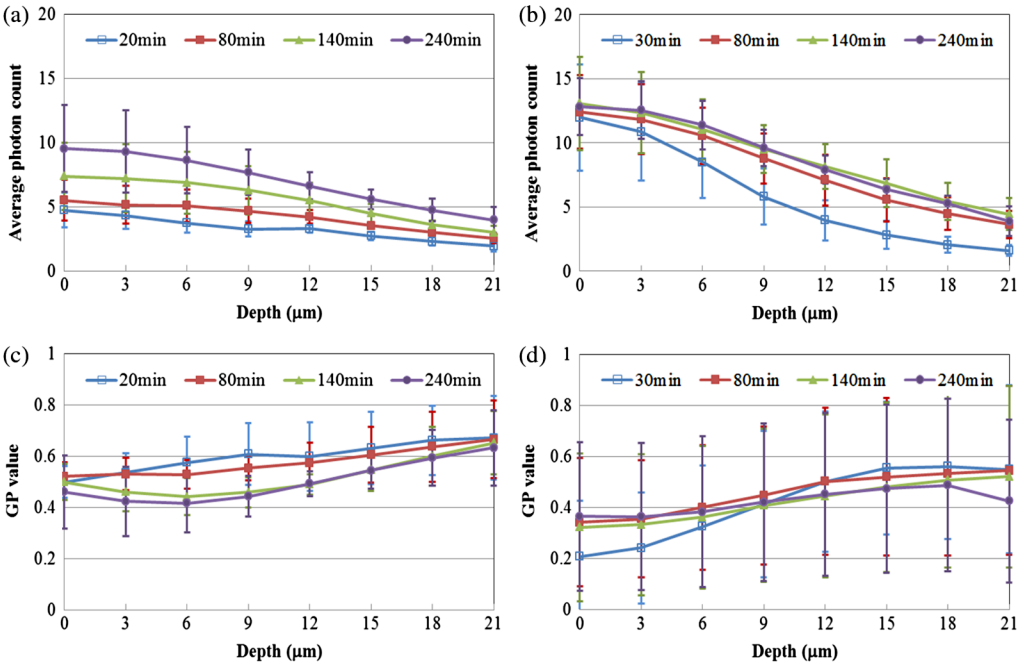

Fig. 5 Quantifications of average SRB intensity and GP values for the intercellular regions. Depth-resolved and time-lapse SRB intensity for the groups without and with oleic acid are, respectively, shown in (a) and (b). *X*-axis is the depth of skin in micrometers and *Y*-axis is the average photon count. (c) and (d) show the results of GP values, respectively, corresponding to (a) and (b) at the same conditions. *X*-axis is the depth of skin in micrometers and *Y*-axis is the GP value. Open squares, dark squares, triangles, and circles of the plots represent the results at time points of 20 (without oleic acid)/30 (with oleic acid), 80, 140, 240 min.

water into the skin. However, Fig. 4(d) of the depth-resolved GP map shows that the group with oleic acid expresses lower values than that of the group without oleic acid, suggesting the oleic acid enhanced SRB permeation to increase polarity of skin tissues. These results are consistent with the fact that oleic acid improves the permeating rates of small molecules in skin tissue by changing packing order of cellular membrane in skin tissues.

Second, since IPR play an important role in transdermal penetration, therefore, in addition to analyzing the overall permeation on SC across the entire image, we also specifically focused on IPR and quantified both of SRB intensity and GP values in IPR at different depths and time points. In the specific analysis of the IPR region, about 10-pixel-wide banded regions were collected, corresponding to boundaries surrounding corneocytes of the selected images. Representative selection of the IPRs in the groups without and with oleic acid treatment is indicated as white-banded regions and, respectively, shown in Figs. 2(a) and 2(b). The plots of average SRB results of IPR in the groups without and with oleic acid, respectively, are shown Figs. 5(a) and 5(b). The results of Fig. 5(a) indicate that the average SRB intensities of IPR at different depths for the group without oleic acid increased with time. The outcome of Fig. 5(a) is similar to that of Fig. 4(a) but shows higher intensity levels in average values, possibly resulting from SRB molecules permeating mostly through IPR for the group without oleic acid. Figure 2(a) also shows that most of the red fluorescence signals emitted by the SRB molecules are located in the boundaries surrounding corneocytes. In the case of Fig. 2 at time point of 80 min and depth of 6 μm, the ratios of the average SRB intensities of IPR to the intracellular regions are 2.67 and 1.93 in the group without and with oleic acid, respectively. Figure 5(b) indicates the group with oleic acid has a faster increasing rate of SRB intensities in IPR than the group without oleic acid. The corresponding plots of average GP values at the same depths and time points of Figs. 5(a) and 5(b) are also displayed in Figs. 5(c) and 5(d). Figure 5(c) shows that for the group without oleic acid, GP values in the IPR tends to decrease with time for every depth. This trend in Fig. 5(c) is in contrast to the results of the overall permeations on SC shown in Fig. 4(c), showing that the decrease of GP value in the IPR for the group without oleic acid corresponds to an increase of polar SRB molecules existing in the IPR. In the group with oleic acid, averaged GP values of both the overall and IPR permeations [Figs. 4(d) and 5(d)] show the same tendency to increase within the first 9-μm depth during the first 80 min, since much higher concentrations of SRB as well as oleic acid temporarily affect the polarity of the upper skin specimen in the beginning of treating the permeation solution. With oleic acid gradually changing the packing order of cellular membrane, SRB molecules could go from IPR (higher concentration) to intracellular regions.

In Figs. 4 and 5, error bars reflect the spread in data from the average results of three specimens in each group. Our results show several features of the permeation of SRB molecules through mouse skin. First, in the group without oleic acid, most of SRB molecules were delivered through IPR. SRB concentrations in IPR also were higher than those in other regions, indicating that SRB has stronger affinity to the IPR. Note that without oleic acid treatment, GP changed with time. This may be due to the fact that water molecules continue to penetrate the skin even in the absence of oleic acid. In comparison, hydrophilic SRB is present in substantially smaller concentrations and should not affect the measured GP values.

In contrast, for both IPR and the overall SC, oleic acid promoted the permeation of SRB through skin and resulted in the elevation of average SRB intensities. Oleic acid significantly

enhanced the permeation of hydrophilic permeation. Since oleic acid can affect the packaging of cellular membrane with time, it can enhance the penetration of aqueous components (such as SRB) from IPR to intracellular regions. In terms of GP values in IPR and the overall SC, a sudden drop within the first 9-μm depth occurred. This is most likely due to the fact that oleic acid enhanced the penetration of aqueous components such as water and SRB molecules.

4 Conclusion

We successfully utilized TPM serving as a noninvasive tool for studying transport dynamics in oleic acid-induced transdermal delivery. In this study, we observed depth-resolved and time-lapse fluorescence images of skin specimen with Lauran and SRB molecules which are, respectively, used as a polarity indicator and transdermal drug. The oleic acid, the permeation enhancer, actually made skin tissues become more permeable to polar molecules such as SRB molecules, corresponding to reduce GP values. The oleic acid promoted the permeation rate of SRB molecules and speeded up the saturation of SRB distributions. The IPRs were more susceptible to oleic acid than the intracellular region, which resulted in higher SRB intensity and lower GP values presented in the IPRs. Spatial and temporal information of transdermal drug delivery achieved by TPM not only provides important messages of drug distributions as well as permeation rates, but also allows an improved understanding of critical effects of chemical enhancer and drugs on skin tissues. Two-photon fluorescence imaging for real-time monitoring transdermal drug delivery shows potential in observations of influences by transdermal drugs and may lead to improved transdermal drug delivery strategies.

Acknowledgments

This study was supported by National Science Council, Taiwan (NSC102-2221-E-002-030-MY3 and NSC 101-2112-M-002-003-MY3), National Health Research Institutes (NHRI-EX102-10041EI), National Taiwan University (NTU-102R7804), the Center for Quantum Science and Engineering of National Taiwan University (CQSE-102R891401), and the World Class University Program at Pusan National University.

References

1. R. O. Potts and M. L. Francoeur, "The influence of stratum corneum morphology on water permeability," *J. Invest. Dermatol.* **96**(4), 495–499 (1991).
2. P. Karande and S. Mitragotri, "Enhancement of transdermal drug delivery via synergistic action of chemicals," *Biochim. Biophys. Acta* **1788**(11), 2362–2373 (2009).
3. P. Karande et al., "Design principles of chemical penetration enhancers for transdermal drug delivery," *Proc. Natl Acad. Sci. U.S.A.* **102**(13), 4688–4693 (2005).
4. M. L. Francoeur, G. M. Golden, and R. O. Potts, "Oleic acid: its effects on stratum corneum in relation to (trans)dermal drug delivery," *Pharm. Res.* **7**(6), 621–627 (1990).
5. B. Yu et al., "In vitro visualization and quantification of oleic acid induced changes in transdermal transport using two-photon fluorescence microscopy," *J. Invest. Dermatol.* **117**(1), 16–25 (2001).
6. B. Yu et al., "Visualization of oleic acid-induced transdermal diffusion pathways using two-photon fluorescence microscopy," *J. Invest. Dermatol.* **120**(3), 448–455 (2003).
7. T. Parasassi, "Laurdan and prodan as polarity-sensitive fluorescent membrane probes," *J. Fluoresc.* **8**(4), 365–373 (1998).
8. T. Parasassi et al., "Two-photon fluorescence microscopy of laurdan generalized polarization domains in model and natural membranes," *Biophys. J.* **72**(6), 2413–2429 (1997).
9. T. Parasassi et al., "Quantitation of lipid phases in phospholipid vesicles by the generalized polarization of Laurdan fluorescence," *Biophys. J.* **60**(1), 179–189 (1991).
10. A. C. Williams and B. W. Barry, "Penetration enhancers," *Adv. Drug Deliv. Rev.* **56**(5), 603–618 (2004).
11. Y. Takeuchi et al., "Skin penetration enhancing action of cis-unsaturated fatty acids with omega-9, and omega-12-chain lengths," *Biol. Pharm. Bull.* **21**(5), 484–491 (1998).
12. G. M. Golden, J. E. McKie, and R. O. Potts, "Role of stratum corneum lipid fluidity in transdermal drug flux," *J. Pharm. Sci.* **76**(1), 25–28 (1987).
13. D. Southwell and B. W. Barry, "Penetration enhancers for human skin: mode of action of 2-pyrrolidone and dimethylformamide on partition and diffusion of model compounds water, n-alcohols, and caffeine," *J. Invest. Dermatol.* **80**(6), 507–514 (1983).
14. A. Ortiz and J. C. Gómez-Fernández, "A differential scanning calorimetry study of the interaction of free fatty acids with phospholipid membranes," *Chem. Phys. Lipids* **45**(1), 75–91 (1987).
15. C. C. Wang et al., "Label-free discrimination of normal and pulmonary cancer tissues using multiphoton fluorescence ratiometric microscopy," *Appl. Phys. Lett.* **97**(4), 043706 (2010).
16. P. So, H. Kim, and I. Kochevar, "Two-photon deep tissue ex vivo imaging of mouse dermal and subcutaneous structures," *Opt. Express* **3**(9), 339–350 (1998).
17. G. M. El Maghraby, B. W. Barry, and A. C. Williams, "Liposomes and skin: from drug delivery to model membranes," *Eur. J. Pharm. Sci.* **34**(4–5), 203–222 (2008).